Walisongo Journal of Chemistry
Walisongo Journal of Chemistry Vol. 8 Issue 2 (2025), 154-176
ISSN: 2621-5985 (online); 2549-385X (print)
DOI: https://doi.org/10.21580/wjc.v8i2.26105

THE POTENTIAL OF CALANONE DERIVATIVES AS ANTILEUKEMIA AGENTS VIA AN IN SILICO APPROACH: MOLECULAR DOCKING AND MOLECULAR DYNAMICS ANALYSIS

Irvan Maulana Firdaus[1], Mutista Hafshah[2], Achmad Akbar[1], Rijal Akhmad Faiz[1], Ponco Iswanto[3], Mochammad Chasani[3], Muhammad Hanafi[4], Eva Vaulina Yulistia Delsy[3]

[1]Senior High School Al Irsyad Al Islamiyyah Boarding School, Purwokerto, Central Java, Indonesia
[2]Department of Chemistry, Faculty of Science and Technology, UIN Walisongo Semarang, Central Java, Indonesia
[3]Department of Chemistry, Faculty of Mathematic and Natural Sciences, Universitas Jenderal Soedirman, Purwokerto, Central Java, Indonesia
[4] Research Center for Chemistry, National Research and Innovation Agency (BRIN), Indonesia

*Corresponding author: Irvanmaulanafirdaus@gmail.com

Abstract

Cancer, particularly leukemia, remains a major global health concern with a high mortality rate, necessitating the development of more effective and selective therapeutic agents. This study evaluated the potential of calanone derivatives as antileukemia agents using an in silico approach. The objectives were to (1) analyze the molecular docking interactions between predicted calanone derivatives and commercial leukemia drugs targeting the Bruton's Tyrosine Kinase (BTK) receptor (PDB ID: 5P9J); (2) predict the ADMET properties (Absorption, Distribution, Metabolism, Excretion, and Toxicity) of the calanone derivatives; and (3) compare the molecular dynamics analysis results of the predicted compounds with those of commercial drugs. The findings revealed that the predicted molecules, including Vaulina2 ((5-hydroxy-2,2-dimethyl-8-oxo-10-phenyl-2H,8H-pyrano[2,3-f]chromen-6-yl)(phenyl)methyl 2-amino-3-(4-hydroxyphenyl)-3-oxopropanoate)), Prediction1 ((8-amino-5-hydroxy-2,2-dimethyl-10-phenyl-2H,8H-pyrano[2,3-f]chromen-6-yl)(phenyl)methanediol)), Prediction2 (6-(dihydroxy(phenyl)methyl)-2,2-dimethyl-10-phenyl-2H,8H-pyrano[2,3-f]chromene-5,8-diol)), Prediction3 (2-amino-9,9-dimethyl-3,7-diphenyl-2,3-dihydro-5H,9H-furo[2,3-f]pyrano[2,3-h]chromen-5-ol)), and Prediction4 (4-(dihydroxy(8-hydroxy-2,2-dimethyl-5-oxo-10-phenyl-6,8-dihydro-2H,5H-pyrano[2,3-f]chromen-6-yl)methyl)benzoic acid)), demonstrated greater stability compared to the reference drug ibrutinib, with Gibbs free energy (ΔG) values of −11.25, −12.50, −10.83, −10.74, and −10.63 kcal/mol, respectively. All compounds also conformed to the predicted ADMET profiles. Molecular dynamics simulations indicated that Vaulina2, Prediction1, and Prediction2 exhibited superior performance based on Root-Mean-Square Deviation (RMSD), Root-Mean-Square Fluctuation (RMSF), Solvent-Accessible Surface Area (SASA), hydrogen bond occupancy, and Molecular Mechanics–Generalized Born Surface Area (MM-GBSA) parameters.

Keywords: *ADMET, calanone, molecular docking, in silico, molecular dynamics*

Introduction

Cancer remains a significant challenge in modern medicine. According to Harris et al. (2021), Hafez et al. (2019), and Kruk et al. (2018), it constitutes a major health problem because it significantly increases mortality rates and has profound social repercussions for families. Cancer is caused by the abnormal multiplication of cells within the body's tissues, which are referred to as malignant tumors (Octavinna et al., 2018). The Ministry of Health of the Republic of Indonesia projected that the number of cancer cases in Indonesia would increase by more than 70% by 2050 if prevention and early detection measures were not strengthened. Correspondingly, approximately 400,000 new cancer cases were detected annually, with the death toll reaching 240,000 (Ministry of Health of the Republic of Indonesia, 2024).

In Indonesia, pediatric populations are primarily affected by hematologic malignancies, which represent the most common type of cancer in children. Leukemia is the most prevalent form among individuals aged 0–19 years, with 3,880 reported cases, surpassing all other cancer types (Tarmizi, 2024; Globocan, 2020). Leukemia is characterized by the proliferation of white blood cells, resulting in an excessive number of abnormal cells (blast cells) in the peripheral blood, thereby impairing the activity of normal blood cells. The disease develops due to the uncontrolled and excessive growth of white blood cells, which prevents other blood cells from performing their normal functions (Iyengar et al., 2023).

Current therapeutic approaches for leukemia include synthetic pharmaceuticals, chemotherapy, radiation therapy, and surgical interventions. Among these, chemotherapy remains the most commonly employed treatment; however, its major drawbacks are high cytotoxicity and non-specificity, both of which adversely affect normal cells. Moreover, the increasing resistance of cancer cells to therapy continues to pose a major obstacle to chemotherapy effectiveness (Lei et al., 2023; Khan et al., 2024). Existing anticancer drugs are further limited by their toxicity toward normal cells (Monika & Remesh, 2012). Researchers are therefore striving to discover new anticancer agents that are both more effective and safer. For instance, doxorubicin has been associated with cardiac toxicity (Santos et al., 2018); cytarabine with neurological side effects (Di et al., 2021); vincristine with peripheral neuropathy (Philips et al., 2021); cyclophosphamide with bladder toxicity (Tsai et al., 2014); daunorubicin with cardiotoxicity (Santos et al., 2018); and fludarabine with severe myelosuppression (Ding et al., 2008). These adverse effects highlight the need for anticancer drugs that are not only potent but also selective and safe. The search for such therapeutic agents is an essential aspect of cancer research aimed at improving the efficacy of pharmacological treatments. However, laboratory-based drug discovery encounters several challenges, including high costs for equipment and skilled labor, as well as the use of complex chemical substances. According to Leelananda and Lindert (2016), the pace and efficiency of laboratory-based drug development are hindered by the extensive research procedures required, which involve testing numerous compounds and employing intricate methodologies.

In the field of medicinal chemistry, computational chemistry plays an essential role, particularly in the design and discovery of new pharmaceuticals, as well as in the theoretical prediction of a drug's chemical properties and biological activities (Alov et al., 2014). The application of sophisticated computational algorithms can significantly reduce research costs and duration, facilitate the design of efficient synthetic pathways, and enhance the optimization of compounds targeting specific proteins (Young, 2009). Computational chemistry encompasses various applications, including molecular docking and molecular dynamics simulations. The molecular docking approach is used to predict the binding conformation of a ligand–protein (receptor)

complex with high accuracy. During molecular docking, the resulting affinity score reflects the binding energy between the ligand and the protein. By comparing the docking scores of different ligands (using the same PDB code, software, and computational settings), it is possible to explain why one molecule exhibits greater potency than another (Purnomo, 2019).

Numerous studies have employed molecular docking to explore drug–cancer cell interactions. For example, organosulfur compounds derived from garlic have been investigated for their interaction with the COX-2 protein in colorectal cancer through molecular docking (Meng et al., 2022; Alrumaihi et al., 2022). Similarly, in silico docking studies have evaluated the anticancer potential of phytol molecules derived from zodiac leaves (Bobe et al., 2020; Gliszczyńska et al., 2021; Anoor et al., 2022), and starfruit leaf compounds for colorectal cancer treatment, including pharmacokinetic and toxicity assessments (Yunarto & Sulistyaningrum, 2017). To complement molecular docking results, molecular dynamics simulations are conducted to analyze the mobility and stability of ligand–receptor complexes over a defined simulation time. These simulations can incorporate physiological parameters such as solvent effects, pressure, pH, and temperature, thus providing a more realistic representation of biological conditions. Examples of docking studies supported by molecular dynamics simulations include the docking and molecular dynamics of furanocoumarin derivatives targeting the estrogen alpha receptor for breast cancer therapy (Meng et al., 2023; Bazmi & Wallin, 2024); investigations of the iron (III)-thiourea metal complex as a potential anticancer agent (Ruswanto et al., 2022; Ruswanto et al., 2023); and docking and molecular dynamics analyses of Monascus sp. compounds for potential cervical cancer treatment (Yuliana et al., 2021).

Calanone, a coumarin derivative isolated from Calophyllum species, has demonstrated cytotoxic activity against L1210 leukemia cell lines, with an IC_{50} value of 59.09 µg/mL (Chasani, 2002). Several synthetic derivatives of calanone have also been evaluated for their antileukemic potential. For instance, octanoate calanil exhibited an IC_{50} of 75.2 µg/mL, isobutyl calanone 105.5 µg/mL, oxycalanone 83.6 µg/mL, kalanone 70 µg/mL, and benzoylphenylalanine ester calanone 52.5 µg/mL. Chasani et al. (2008) synthesized ethylenediamine calanone, which showed enhanced potency with an IC_{50} of 39.57 µg/mL. Further structural modification, such as hydration of the C7–C8 double bond (Chasani et al., 2010), yielded a compound with a 4.72% (w/w) recovery and an IC_{50} of 45.64 µg/mL. In 2011, 2,4,6-trinitrophenylhydrazone calanone was synthesized with a 5.13% (w/w) yield and an IC_{50} of 47.69 µg/mL. However, all these findings were derived from in vitro assays against leukemia cell lines; to date, no in vivo or clinical studies have been reported evaluating calanone or its derivatives for leukemia treatment.

In addition, Iswanto et al. (2011) investigated calanone derivatives using computational and synthetic approaches. Their findings revealed that the computationally predicted calanone derivatives exhibited enhanced inhibitory activity against leukemia cells. Among these derivatives, gemdiol calanone demonstrated an IC_{50} value of 57.78 µg/mL, 2,4-dinitrophenylhydrazone calanone showed an IC_{50} value of 30.94 µg/mL, and 2,4,6-trinitrophenylhydrazone calanone exhibited the highest potency with an IC_{50} value of 18.96 µg/mL. A subsequent study by Vaulina et al. (2012) expanded upon this research by conducting a quantitative structure–activity relationship (QSAR) analysis of calanone derivatives as inhibitors of L1210 leukemia cells, further advancing computational investigations in this field. Through this analysis, several novel calanone derivatives with promising anticancer potential were identified, namely 1) Vaulina1 (2-amino-3-((5-hydroxy-2,2-dimethyl-8-oxo-10-phenyl-2H,8H-pyrano[2,3-f]chromen-6-yl)(phenyl)methoxy)-3-oxopropanoic acid); 2) Vaulina2 ((5-hydroxy-2,2-dimethyl-8-

oxo-10-phenyl-2H,8H-pyrano[2,3-f]chromen-6-yl)(phenyl)methyl 2-amino-3-(4-hydroxyphenyl)-3-oxopropanoate); 3) Vaulina3 ((5-hydroxy-2,2-dimethyl-8-oxo-10-phenyl-2H,8H-pyrano[2,3-f]chromen-6-yl)(phenyl)methyl 2-amino-5-hydroxy-4-oxohexanoate); and 4) Vaulina4 ((5-hydroxy-2,2-dimethyl-8-oxo-10-phenyl-2H,8H-pyrano[2,3-f]chromen-6-yl)(phenyl)methyl 2-amino-4-oxo-5-phenylpentanoate)). These compounds displayed IC_{50} values of 26.44, 25.61, 27.05, and 23.01 µg/mL, respectively, when tested against L1210 leukemia cells. Nonetheless, the research by Vaulina et al. (2012) was limited to theoretical predictions derived from QSAR modeling. The study did not incorporate molecular docking or molecular dynamics simulations; thus, the binding mechanisms and interaction stability of these predicted compounds remain to be verified. Therefore, the present study aimed to extend this line of research by employing the calanone derivatives proposed by Vaulina et al. (2012) and newly modified calanone derivatives to evaluate their potential as leukemia inhibitors through in silico methods. Molecular docking and molecular dynamics simulations were performed using AutoDock Vina and GROMACS, respectively, to elucidate the binding affinities, interaction stability, and dynamic behavior of these compounds against the target leukemia receptor.

Experimental Section

Instruments and Substances

This study was conducted using a workstation equipped with an Intel® Core™ i7 CPU, 32 GB of RAM, and the Windows 11 operating system. The software tools employed included Discovery Studio 2021 Client (BIOVIA, Dassault Systèmes, 2021), AutoDockTools 1.5.7 (Morris et al., 2009), AutoDock Vina (Trott & Olson, 2010), Vina Split (AutoDock Vina utility), Windows PowerShell, Avogadro (Hanwell et al., 2012), MarvinSketch (ChemAxon, 2023), and the Linux Ubuntu 22.04.4 subsystem. Molecular dynamics simulations were performed using GROMACS (Abraham et al., 2015), while visualization and trajectory analyses were conducted with VMD 1.9 (Humphrey et al., 1996) and UCSF Chimera 1.17.3 (Pettersen et al., 2004). This study utilized compound data of predicted calanone derivatives provided by Vaulina et al. (2012), along with several modified derivative predictions. The compounds designed by Vaulina et al. (2012) were referred to as 1) Vaulina1: 2-amino-3-((5-hydroxy-2,2-dimethyl-8-oxo-10-phenyl-2H,8H-pyrano[2,3-f]chromen-6-yl)(phenyl)methoxy)-3-oxopropanoic acid; 2) Vaulina2: (5-hydroxy-2,2-dimethyl-8-oxo-10-phenyl-2H,8H-pyrano[2,3-f]chromen-6-yl)(phenyl)methyl 2-amino-3-(4-hydroxyphenyl)-3-oxopropanoate; 3) Vaulina3: (5-hydroxy-2,2-dimethyl-8-oxo-10-phenyl-2H,8H-pyrano[2,3-f]chromen-6-yl)(phenyl)methyl 2-amino-5-hydroxy-4-oxohexanoate; and 4) Vaulina4: (5-hydroxy-2,2-dimethyl-8-oxo-10-phenyl-2H,8H-pyrano[2,3-f]chromen-6-yl)(phenyl)methyl 2-amino-4-oxo-5-phenylpentanoate. Meanwhile, the modified or newly predicted derivatives were referred to as 1) Prediction1: (8-amino-5-hydroxy-2,2-dimethyl-10-phenyl-2H,8H-pyrano[2,3-f]chromen-6-yl)(phenyl)methanediol; 2) Prediction2: 6-(dihydroxy(phenyl)methyl)-2,2-dimethyl-10-phenyl-2H,8H-pyrano[2,3-f]chromene-5,8-diol; 3) Prediction3: 2-amino-9,9-dimethyl-3,7-diphenyl-2,3-dihydro-5H,9H-furo[2,3-f]pyrano[2,3-h]chromen-5-ol; and 4) Prediction4: 4-(dihydroxy(8-hydroxy-2,2-dimethyl-5-oxo-10-phenyl-6,8-dihydro-2H,5H-pyrano[2,3-f]chromen-6-yl)methyl)benzoic acid (see Figure 1). The protein data used in this study were obtained from the Protein Data Bank (PDB ID: 5P9J) and are accessible at https://www.rcsb.org.

Antileukemia Activity Prediction

The antileukemia activity of the selected compounds was predicted using PASS Online (http://www.way2drug.com/passonline/) (Lagunin et al., 2000). Each compound was submitted in the form of canonical SMILES, and the biological activity spectrum was expressed as the probability of activity (Pa) and inactivity (Pi). Compounds with a Pa

 | ISSN 2621-5985 (online) | ISSN 2549-385X (print)
Volume 8, Nomor 2, 2025

value greater than 0.3 were considered to have potential in silico antileukemia activity and were subjected to further molecular docking simulations. This cutoff threshold has been consistently applied in previous studies employing PASS prediction for natural product screening (Akinmoladun et al., 2020; Wicaksono et al., 2022).

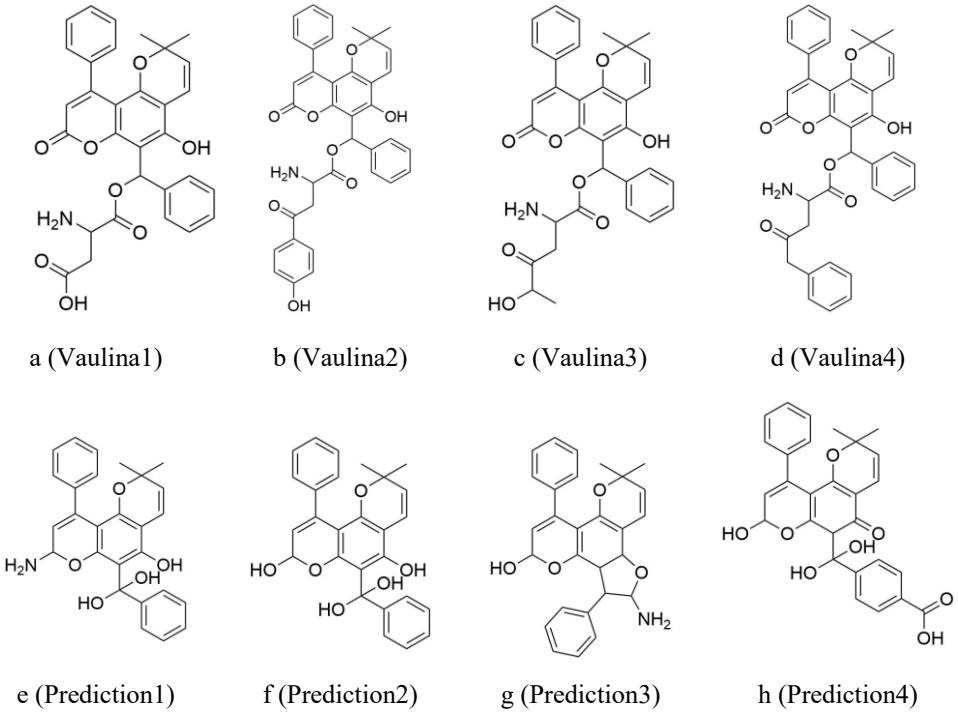

Figure 1. Predicted structures of calanone derivative compounds.

Preparation of Protein and Ligand

The crystal structure of the target protein (PDB ID: 5P9J) was retrieved from the RCSB Protein Data Bank (https://www.rcsb.org). Protein preparation was performed using Discovery Studio 2021 Client by removing all water molecules and the native ligand to prevent undesired interactions during docking. The processed protein structure was saved in PDB format for subsequent simulations, while the extracted native ligand was stored separately for use as a reference compound. All protein and ligand preparation steps followed the software's default parameters with no additional constraints applied (Purnawan, 2022).

Docking of Predicted Compounds

The protein structure (PDB ID: 5P9J) was retrieved from the RCSB Protein Data Bank. All water molecules and native ligands were removed, followed by the addition of polar hydrogen atoms and assignment of Gasteiger charges prior to conversion into PDBQT format. Ligands, including the native ligand and the predicted calanone derivatives, were geometry-optimized using the MMFF94 force field in Avogadro. Polar hydrogens were added, and torsional flexibility was assigned using the "fewest rotatable bonds" setting to reduce conformational redundancy. Molecular docking simulations were performed using AutoDock Vina. The docking grid was centered on the native ligand binding site, with a grid box encompassing the binding pocket at a grid spacing of 1.0 Å. The number of modes was set to 10 (default), while the exhaustiveness parameter was increased to 32 to enhance sampling accuracy. Validation of the docking

protocol was conducted through re-docking of the native ligand, where a Root-Mean-Square Deviation (RMSD) value below 2 Å indicated a reliable docking configuration. Docking scores were expressed as binding free energies (kcal/mol). Predicted compounds exhibiting favorable binding affinities were further examined for key amino acid interactions using Discovery Studio Visualizer (Purnawan, 2022).

Analysis of Adsorption, Distribution, Metabolism, Excretion, and Toxicity

Pharmacokinetic properties of the compounds were predicted using pkCSM (https://biosig.lab.uq.edu.au/pkcsm/). Each compound structure was submitted to generate parameters representing absorption, distribution, metabolism, excretion, and toxicity (ADMET) profiles. Absorption parameters were evaluated using Human Intestinal Absorption (HIA) and Caco-2 permeability values. Distribution properties were determined from Plasma Protein Binding (PPB) and Blood–Brain Barrier (BBB) penetration values. Additional parameters concerning metabolism, excretion, and toxicity were also analyzed to provide a comprehensive pharmacokinetic prediction (Sagita et al., 2021).

Molecular Dynamics Simulation

Molecular dynamics simulations were performed for the three most promising predicted compounds based on docking results. The procedure involved sequential preparation of input files, including ions.mdp, em.mdp, nvt.mdp, npt.mdp, and md.mdp. The workflow comprised receptor–ligand topology generation, ion addition, energy minimization, temperature and pressure equilibration, and production simulation using GROMACS. Subsequent analyses and visualizations were conducted to evaluate RMSD, Root-Mean-Square Fluctuation (RMSF), hydrogen bond occupancy, and Molecular Mechanics–Generalized Born Surface Area (MM-GBSA) binding free energy (Purnawan, 2022).

Results and Discussion

Antileukemia Activity Prediction

The bioactivity prediction conducted using PASS Online indicated that all tested compounds exhibited Pa values within the range of 0.3–0.7, suggesting their potential as antineoplastic agents and suitability for further molecular docking analysis. Compounds within this range are considered in silico candidates, though their probability of experimental activity remains relatively low (Lagunin et al., 2000). One predicted compound (Prediction3) demonstrated a Pa value of 0.818 with Pi = 0.010, reflecting a high confidence level in its biological activity. According to PASS evaluation criteria, compounds with Pa > 0.7 are regarded as highly promising for relevant experimental validation (Akinmoladun et al., 2020). While PASS provides predictions under the general category of “antineoplastic,” this term broadly encompasses agents active against neoplastic (cancerous) cells. In the context of this study, the interpretation was specifically focused on antileukemia potential, as the target receptor and biological mechanisms were associated with leukemia. These findings align with previous research by Wicaksono et al. (2022), which demonstrated that metabolites from endemic plants with high Pa values predicted by PASS could later be confirmed as anticancer agents through molecular docking and subsequent biological validation. Therefore, all compounds investigated in this study qualified as candidates for molecular docking analysis, with Prediction3 emerging as the most promising lead compound for antileukemia activity prediction.

Table 1. PASS Online Prediction Results of Antileukemia Activity for Vaulina and Predicted

Compound	IUPAC Name	Pa
Vaulina1	2-amino-3-((5-hydroxy-2,2-dimethyl-8-oxo-10-phenyl-2H,8H-pyrano[2,3-f]chromen-6-yl)(phenyl)methoxy)-3-oxopropanoic acid	0.533
Vaulina2	(5-hydroxy-2,2-dimethyl-8-oxo-10-phenyl-2H,8H-pyrano[2,3-f]chromen-6-yl)(phenyl)methyl 2-amino-3-(4-hydroxyphenyl)-3-oxopropanoate	0.620
Vaulina3	(5-hydroxy-2,2-dimethyl-8-oxo-10-phenyl-2H,8H-pyrano[2,3-f]chromen-6-yl)(phenyl)methyl 2-amino-5-hydroxy-4-oxohexanoate	0.502
Vaulina4	(5-hydroxy-2,2-dimethyl-8-oxo-10-phenyl-2H,8H-pyrano[2,3-f]chromen-6-yl)(phenyl)methyl 2-amino-4-oxo-5-phenylpentanoate	0.488
Prediction1	(8-amino-5-hydroxy-2,2-dimethyl-10-phenyl-2H,8H-pyrano[2,3-f]chromen-6-yl)(phenyl)methanediol	0.742
Prediction2	6-(dihydroxy(phenyl)methyl)-2,2-dimethyl-10-phenyl-2H,8H-pyrano[2,3-f]chromene-5,8-diol	0.746
Prediction3	2-amino-9,9-dimethyl-3,7-diphenyl-2,3-dihydro-5H,9H-furo[2,3-f]pyrano[2,3-h]chromen-5-ol	0.818
Prediction4	4-(dihydroxy(8-hydroxy-2,2-dimethyl-5-oxo-10-phenyl-6,8-dihydro-2H,5H-pyrano[2,3-f]chromen-6-yl)methyl)benzoic acid	0.603

Receptor Examination

The molecular docking procedure began with the preparation of the receptor's macromolecular structure, obtained from the Protein Data Bank (PDB) at https://www.rcsb.org/. This study examined a receptor associated with hematological malignancies that was linked to the Bruton's Tyrosine Kinase (BTK) pathway, designated under PDB ID: 5P9J. The selected protein receptor must satisfy several structural criteria, including a resolution ≤ 2 Ångström and a Ramachandran plot value showing at least 90% residues in the "most favored regions" (Ramadhani et al., 2021). The parameters of the BTK receptor are summarized in Table 2. The data indicate that the BTK receptor (PDB ID: 5P9J) had a resolution of 1.08 Å, reflecting a high-quality structural model. According to Putra (2022), a lower resolution value signifies a more refined receptor structure with improved accuracy. Similarly, Reynaldi and Setiawansyah (2022) emphasize that receptors derived from Homo sapiens and determined via X-ray crystallography are considered reliable for computational studies. The receptor structure used in this study met these criteria, as it was determined using X-ray crystallography and validated internally by the RCSB PDB. The corresponding validation report can be accessed directly through the PDB 5P9J dashboard at https://www.rcsb.org/structure/5P9J. Therefore, an independent Ramachandran plot analysis was not deemed necessary.

Table 2. Specifications of Bruton's Tyrosine Kinase Receptor

Macromolecule	PDB ID	Resolution (Å)	Diffraction Method	Species	Ligand
BTK	5P9J	1.08	X-ray	*Homo sapiens*	ibrutinib

Preparation of Bruton's Tyrosine Kinase Receptor

The BTK receptor (PDB ID: 5P9J) was prepared by removing solvent molecules, including water, as well as other non-essential residues from the protein structure using Discovery Studio 2021. This step is crucial to prevent unwanted interactions during the docking process (Sari et al., 2020). The preparation stage also involved separating the protein structure from its native ligand to define the ligand-binding pocket of the target protein (Susanti et al., 2019). Both the protein and native ligand structures were then saved in .pdb format. The native ligand was subsequently optimized using Avogadro software, employing the Molecular Mechanics method with the MMFF94 force field to achieve a lower energy state and a stable molecular conformation. Energy minimization is essential for optimizing atomic positions, reducing interatomic forces and steric energy toward zero, thereby improving the reliability of docking scores (Baissantz et al., 2010). Figure 2 displays the structures of the protein and the native ligand following preparation. Subsequently, the native ligand and the receptor were enriched with polar hydrogen atoms and assigned Gasteiger charges using AutoDock Tools, and then saved in .pdbqt format. The inclusion of polar hydrogens can enhance the identification of potential hydrogen-bond interactions, whereas the application of Gasteiger charges ensures that the docking conditions reflect physiological pH, leading to more accurate binding energy calculations (Kolina et al., 2019).

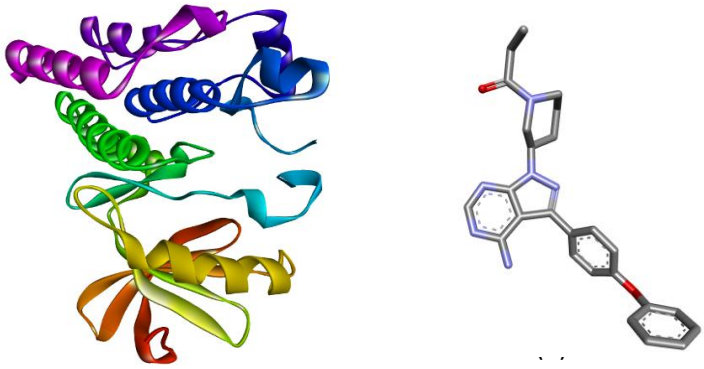

(a) (b)

Figure 2. 3D structures of (a) protein and (b) native ligand of Bruton's Tyrosine Kinase (PDB ID: 5P9J).

Table 3. Docking Results of the Native Ligand and Protein

Receptor	ΔG Binding Energy (kcal/mol)	RMSD (Å)	RMSD Visualization
Bruton's Tyrosine Kinase (PDB ID: 5P9J)	-10.92	0.538	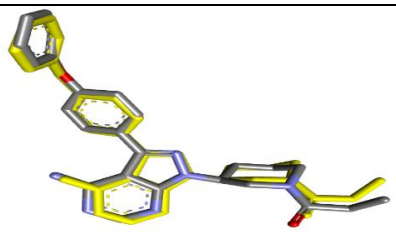

Assessment of Grid Box and Root-Mean-Square Deviation

The initial phase in validating the molecular docking protocol involved configuring the grid box, which defined the spatial boundaries for the ligand's movement and assisted in identifying the active binding site of the protein. The grid box represents the interaction region between the native ligand and the amino acid residues of the target protein (Rachmania et al., 2016). Analysis of the grid box for the BTK receptor (PDB ID: 5P9J) and its native ligand revealed that the ligand was positioned centrally within the grid. The grid spacing was set to 1.0 Å, with dimensions of 12 × 8 × 14 points, and center coordinates of X = 19.741, Y = 8.387, and Z = 4.538. Figure 3 illustrates the location of the native ligand within the grid box.

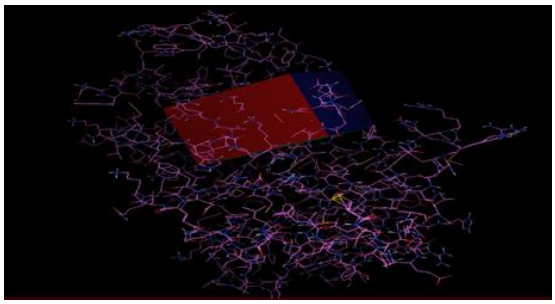

Figure 3. Location of the native ligand within the grid box.

The next step in docking validation was to calculate the RMSD by re-docking the native ligand with its corresponding protein using AutoDock Vina. The RMSD value measures the deviation between the predicted docked pose and the experimentally observed 3D conformation of the ligand (Rachmania, 2019). In this study, AutoDock Vina was employed for molecular docking, and RMSD calculations were visualized using Discovery Studio. The resulting binding energy and RMSD values are summarized in Table 3. The RMSD values obtained fall within the acceptable range, as Purnomo (2024) states that RMSD values must be below 2 Å to validate docking reliability. A lower RMSD indicates higher accuracy of the docking protocol, which can then be optimized for virtual screening to identify novel receptor inhibitors (Purnomo, 2011). The interactions between the native ligand and amino acid residues were visualized using Discovery Studio, as depicted in Figure 4.

The predicted binding pose of the native ligand exhibited a very low RMSD value of 0.538 Å when compared with the co-crystallized ligand, indicating an excellent overlap with the experimentally determined binding conformation. RMSD values below 2.0 Å are generally accepted as indicative of reliable docking predictions and good reproduction of experimental binding modes (Hevener et al., 2009). Key hydrogen bond interactions were observed with Cys481, Ser538, and Glu475, while hydrophobic contacts occurred with Val416, Leu408, and Met477. These interactions are consistent with those reported in previous crystallographic analyses (Trott & Olson, 2010; Morris et al., 2009). These findings demonstrate that the docking protocol employed in this study was robust and capable of accurately reproducing experimentally observed ligand–protein interactions.

Table 4. Molecular Docking Results of Compounds with Bruton's Tyrosine Kinase Receptor (PDB ID: 5P9J)

No	Compound Name	ΔG Binding Energy (kcal/mol)	Binding with Amino Acids	
			Hydrogen Bonds	Hydrophobic Interactions
1	Native ligand	-10.92	Cys A:481, Met A:477,	Gly A:409, Gly A:480, Thr A:410, Leu A:528, Leu A:408, Tyr A:476, Ala A:428, Thr A:474, Ser A:538, Leu A:542, Phe A:540, Asp A:539,

No	Compound Name	ΔG Binding Energy (kcal/mol)	Binding with Amino Acids	
			Hydrogen Bonds	Hydrophobic Interactions
			Glu A:475	Met A:449, Val A:458, Ile A:472, Lys A:430, Val A:416, Asn A:484
2	Ibrutinib	-10.40	Met A:477, Glu A:475, Thr A:474	Gly A:409, Gly A:480, Leu A:528, Leu A:408, Tyr A:476, Ala A:428, Val A:458, Ser A:538, Ile A:472, Leu A:542, Met A:449, Phe A:540, Asp A:539, Leu A:460, Lys A:430, Val A:416, Cys A:481, Arg A:525
3	Vaulina1	-6.38	Ser A:538, Asp A:539, Lys A:430	Leu A:408, Val A:416, Leu A:528, Gln A:412, Asn A:526, Gly A:411, Phe A:413, Ala A:428, Thr A:474, Val A:458, Arg A:525, Cys A:481, Gly A:480, Met A:477, Asn A:484
4	Vaulina2	-11.25	Asp A:539, Ser A:538	Gln A:412, Gly A:411, Thr A:410, Gly A:409, Val A:416, Leu A:542, Phe A:540, Met A:449, Thr A:474, Ile A:472, Leu A:408, Val A:458, Ala A:428, Glu A:475, Tyr A:476, Leu A:528, Met A:477, Lys A:430, Asn A:526, Arg A:525
5	Vaulina3	-6.92	Ser A:538, Lys A:430, Asp A:539	Cys A:481, Gly A:480, Val A:416, Leu A:408, Leu A:528, Glu A:475, Tyr A:476, Ala A:428, Met A:477, Thr A:474, Val A:458, Leu A:460, Met A:449, Leu A:542, Ile A:472, Gly A:411, Arg A:525, Gly A:409, Asn A:484
6	Vaulina4	-8.32	Ser A:538, Thr A:474, Asp A:539	Arg A:525, Cys A:481, Asn A:526, Leu A:528, Glu A:475, Ala A:428, Val A:458, Met A:477, Tyr A:476, Ile A:472, Met A:449, Phe A:540, Leu A:542, Lys A:430, Leu A:408, Val A:416, Gly A:409, Gly A:411
7	Prediction1	-12.50	Asp A:539	Gly A:480, Cys A:481, Gly A:409, Leu A:408, Tyr A:476, Met A:477, Glu A:475, Ala A:428, Thr A:474, Val A:458, Ile A:472, Leu A:542, Lys A:430, Ser A:538, Val A:416, Leu A:528, Gly A:411, Arg A:525
8	Prediction2	-10.83	Ser A:538, Thr A:474, Met A:477	Gly A:411, Arg A:525, Val A:458, Asp A:539, Lys A:430, Leu A:528, Ala A:428, Ile A:472, Val A:416, Tyr A:476, Leu A:408, Gly A:480, Cys A:481, Gly A:409

No	Compound Name	ΔG Binding Energy (kcal/mol)	Binding with Amino Acids	
			Hydrogen Bonds	Hydrophobic Interactions
9	Prediction3	-10.74	Glu A:475, Lys A:430, Asn A:526	Ser A:538, Asp A:539, Ile A:472, Thr A:474, Leu A:542, Arg A:525, Cys A:481, Gly A:480, Leu A:408, Leu A:528, Met A:477, Val A:416, Ala A:428, Val A:458
10	Prediction4	-10.63	Asp A:539, Thr A:474, Ser A:538	Met A:449, Leu A:460, Val A:458, Phe A:540, Leu A:542, Ile A:472, Lys A:430, Cys A:481, Gly A:409, Gly A:480, Leu A:408, Met A:477, Glu A:475, Tyr A:476, Val A:416, Leu A:528, Ala A:428

Molecular Docking and Visualization of Docking Outcomes

Molecular docking was performed for eight compounds (see Figure 1) against the BTK receptor (PDB ID: 5P9J). The docking analysis was carried out using AutoDock Vina, focusing on the conformations of each compound that exhibited the lowest binding energy (ΔG). The purpose of molecular docking was to elucidate the binding conformation and molecular interactions of the test compounds within the active site of the target protein receptor (Meng et al., 2022; Mohanty & Mohanty, 2023; Trott & Olson, 2010). The grid box configuration, defining the region where ligand interactions occur, was consistent with that used during the re-docking validation stage. It comprised dimensions of 12 × 8 × 14 points, centered at coordinates X = 19.741, Y = 8.387, and Z = 4.538. Table 4 presents the molecular docking results, including the binding affinities and amino acid interactions of each compound with the BTK receptor.

The molecular docking simulations summarized in Table 4 present the ΔG values and the interacting amino acid residues for each compound against the Bruton's Tyrosine Kinase (BTK) receptor (PDB ID: 5P9J). According to Mardianingrum et al. (2021), compounds that exhibit lower Gibbs free energy possess stronger and more stable interactions with their target receptor. As shown in Table 4, the predicted compounds Vaulina2, Prediction1, Prediction2, Prediction3, and Prediction4 demonstrate lower (more negative) ΔG values compared to the commercial drug ibrutinib, indicating greater thermodynamic stability and stronger binding affinities toward BTK. These findings suggest that these compounds hold potential as novel BTK inhibitors with prospective antileukemia activity. The strong binding affinities observed for Vaulina2 and the Prediction series compounds are likely attributed to multiple hydrogen bond interactions, which play a critical role in stabilizing ligand–receptor complexes. Hydrogen bonds are specific and directional interactions that enhance a ligand's affinity by forming electrostatic attractions between hydrogen donors and acceptors within the receptor's active site (Muttaqin, 2019). The receptor–ligand complexes were visualized using Discovery Studio, as shown in Figure 4. In these visualizations, dashed lines represent various types of non-covalent interactions, including hydrogen bonds, electrostatic forces, hydrophobic contacts, halogen interactions, and van der Waals forces (Bazmi & Wallin, 2024; Wang et al., 2008). The detailed interactions between Vaulina2, Prediction1, Prediction2, Prediction3, and Prediction4 with the BTK receptor are depicted in Figure 5.

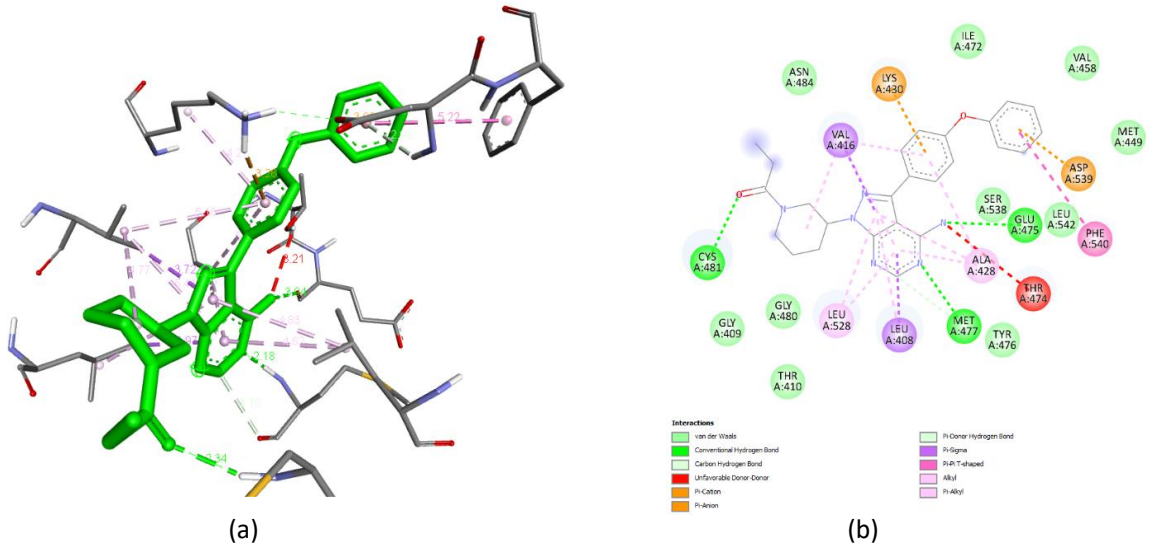

(a) (b)

Figure 4. (a) Visualization of docking results; (b) Interaction between the native ligand and amino acid residues.

ADMET Analysis: Absorption, Distribution, Metabolism, Excretion, and Toxicity

The subsequent phase of this study involved an ADMET evaluation to assess the pharmacokinetic properties and safety profiles of the predicted compounds. The analysis was performed using the web-based pkCSM platform available at https://biosig.lab.uq.edu.au/pkcsm/. The parameters analyzed included HIA, which predicts the extent to which an active compound can be absorbed in the human intestine. The HIA results revealed three levels of absorption: moderate absorption (20–70%) for Prediction4, and high absorption (70–100%) for the other compounds, namely ibrutinib, Prediction1, Prediction2, Prediction3, and Vaulina2 (Sagita et al., 2021). To further assess oral bioavailability, the Caco-2 cell permeability test was used to predict the absorption or transport of orally administered drugs across the intestinal epithelium. The Caco-2 analysis results indicated that ibrutinib, Vaulina2, Prediction3, and Prediction4 exhibited moderate permeability (0.5–1 mm/s), while Prediction1 and Prediction2 were categorized as highly permeable (>1 mm/s). The BBB penetration parameter was analyzed to evaluate each compound's ability to cross the blood–brain barrier. The results demonstrated that Prediction3 was capable of BBB penetration (>0.3), whereas the remaining compounds, ibrutinib, Vaulina2, Prediction1, Prediction2, and Prediction4, were classified as non-permeable (<−1) (Pires et al., 2015). These findings suggest that the latter compounds exhibited favorable pharmacological selectivity, remaining largely restricted to peripheral tissues rather than entering the central nervous system (see Table 5).

The next parameter examined was metabolism, focusing on the inhibitory effects of the compounds on Cytochrome P450 (CYP) enzymes, specifically CYP2C19, CYP2C9, CYP2D6, and CYP3A4. Inhibition of CYP enzymes might interfere with drug metabolism, potentially increasing plasma drug concentrations and leading to adverse effects. The analysis revealed that ibrutinib inhibited three CYP isoenzymes (CYP2C19, CYP2C9, and CYP3A4), whereas the predicted compounds inhibited only one or two of these enzymes. This finding indicates that ibrutinib may present a higher risk of metabolic interaction compared with Vaulina2, Prediction1, Prediction2, Prediction3, and Prediction4. The excretion parameter was evaluated using total clearance as an indicator. The findings showed that ibrutinib, Vaulina2, Prediction1, and Prediction3 displayed favorable clearance rates, while Prediction2 and Prediction4 exhibited lower clearance,

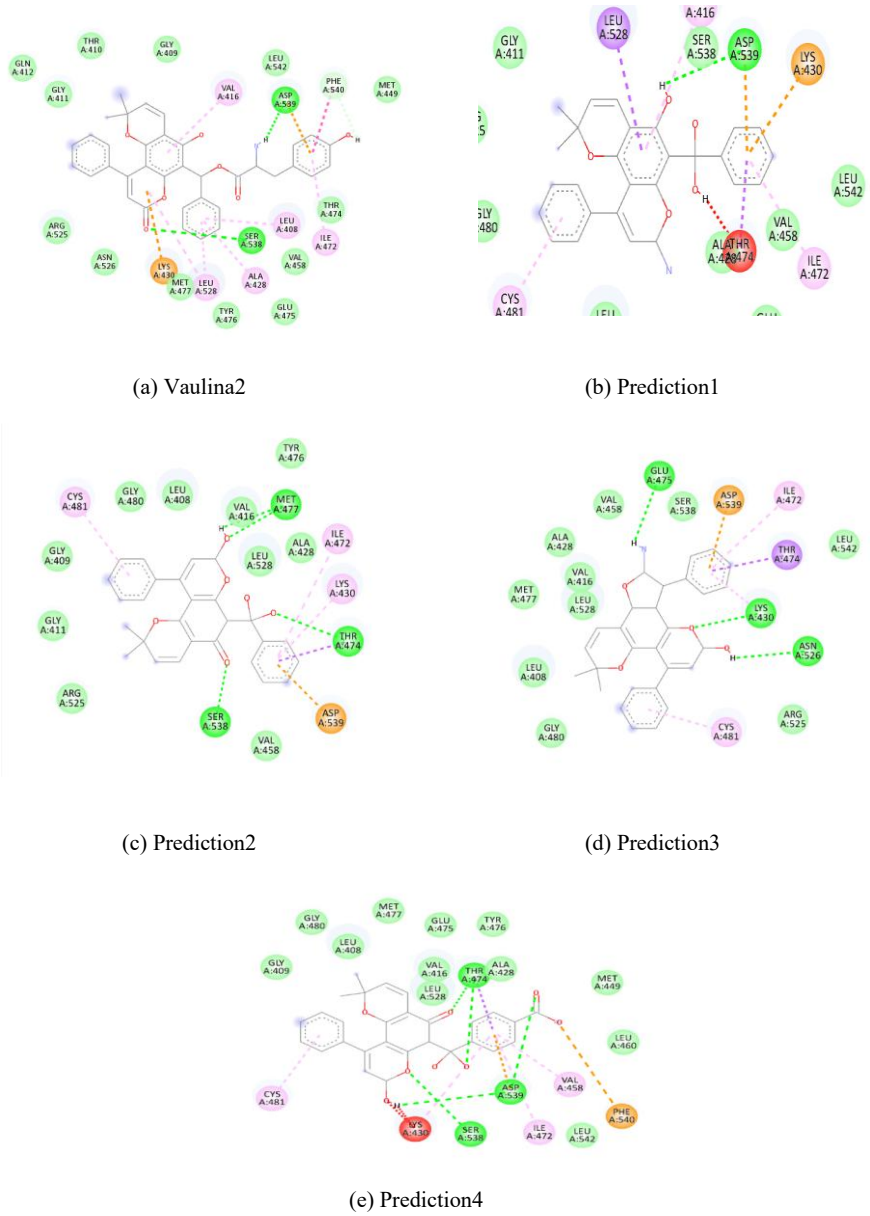

(a) Vaulina2 (b) Prediction1

(c) Prediction2 (d) Prediction3

(e) Prediction4

Figure 5. Interactions between amino acid residues and the predicted compounds: (a) Vaulina2, (b) Prediction1, (c) Prediction2, (d) Prediction3, (e) Prediction4. Color codes: green lines represent conventional hydrogen bonds; light green lines represent carbon–h

suggesting longer retention times in the body (Pires et al., 2015). Finally, the toxicity parameter was assessed using the Ames test, which predicts genotoxicity and potential carcinogenic effects. The analysis indicated that neither ibrutinib nor the predicted compounds (Vaulina2, Prediction1, Prediction2, Prediction3, and Prediction4) exhibited mutagenic or carcinogenic properties, confirming their non-carcinogenic nature.

Table 5. ADMET Parameters of Ibrutinib and Predicted Compounds

No	Compound	Parameter								
		Absorption		Distribution	Metabolism				Excretion	Toxicity
		HIA (%)	Caco-2 (mm/s)	BBB (%)	CYP2C19 Inhibition	CYP2C9 Inhibition	CYP2D6 Inhibition	CYP3A4 Inhibition	Total Clearance	Ames Test
1	Ibrutinib	97.7	0.704	-0.902	yes	yes	no	yes	0.601	no

2	Vaulina2	100.0	0.530	-1.103	no	no	no	yes	0.475	no
3	Prediction1	86.9	1.064	-1.026	yes	yes	no	no	0.661	no
4	Prediction2	88.0	1.145	-0.850	no	yes	no	no	0.036	no
5	Prediction3	93.3	0.658	0.305	yes	no	no	yes	0.469	no
6	Prediction4	67.7	0.995	-1.230	no	no	no	no	0.095	no

Molecular Dynamics Analysis

Molecular dynamics simulations were conducted on the BTK receptor (PDB ID: 5P9J) in complex with the commercial drug ibrutinib and the predicted compounds Vaulina2, Prediction1, Prediction2, Prediction3, and Prediction4, using GROMACS software. The objective of this analysis was to evaluate the stability and conformational behavior of the protein–ligand complexes under conditions approximating human physiological environments over a defined simulation period (Muttaqin, 2019). The preparation phase of the molecular dynamics simulation involved the generation of topology and coordinate files for the ligands and the receptor, which were subsequently assembled into protein–ligand complexes. The simulation workflow consisted of several stages: 1) Solvation of the protein–ligand complex within a cubic box containing explicit water molecules; 2) Neutralization of the system using counter-ions (Na^+ and Cl^-) to achieve charge balance; 3) Energy minimization to eliminate atomic clashes and optimize hydrogen-bond geometry; 4) Equilibration to maintain constant temperature, pressure, and volume; and 5) Production simulation, during which the dynamic behavior of the system was recorded (Karplus, 2002; Van der Spoel et al., 2001). The molecular dynamics simulations were performed for 10 ns for both ibrutinib and the predicted compounds. The calculated parameters included RMSD, RMSF, Solvent-Accessible Surface Area (SASA), hydrogen bond occupancy, and MM-GBSA binding energy estimations.

RMSD (Root Mean Square Deviation)

RMSD is a commonly used quantitative metric for assessing structural deviations and conformational changes in molecular dynamics trajectories (Sinha et al., 2023). In the context of this study, RMSD analysis was employed to determine the degree of conformational deviation within each protein–ligand complex over time (Muttaqin, 2019). Figure 6 presents the RMSD profiles obtained from the molecular dynamics simulations. The trajectories show that the RMSD values of the complexes stabilized between approximately 0.2 ns and 10 ns, with both the protein and ligand exhibiting only minor fluctuations, suggesting that the systems achieved equilibrium stability. Throughout the simulation, RMSD fluctuations did not exceed 0.1 nm, indicating consistent and stable ligand–receptor interactions. The compounds demonstrating the most stable RMSD profiles were ibrutinib, Vaulina2, Prediction1, Prediction2, and Prediction4. Conversely, Prediction3 displayed greater RMSD variation, suggesting higher conformational flexibility, likely due to structural rearrangements within the binding pocket during interaction with the receptor. Therefore, the RMSD analysis indicates that most predicted compounds formed stable complexes with BTK, with Prediction3 showing comparatively less structural stability (see Figure 6).

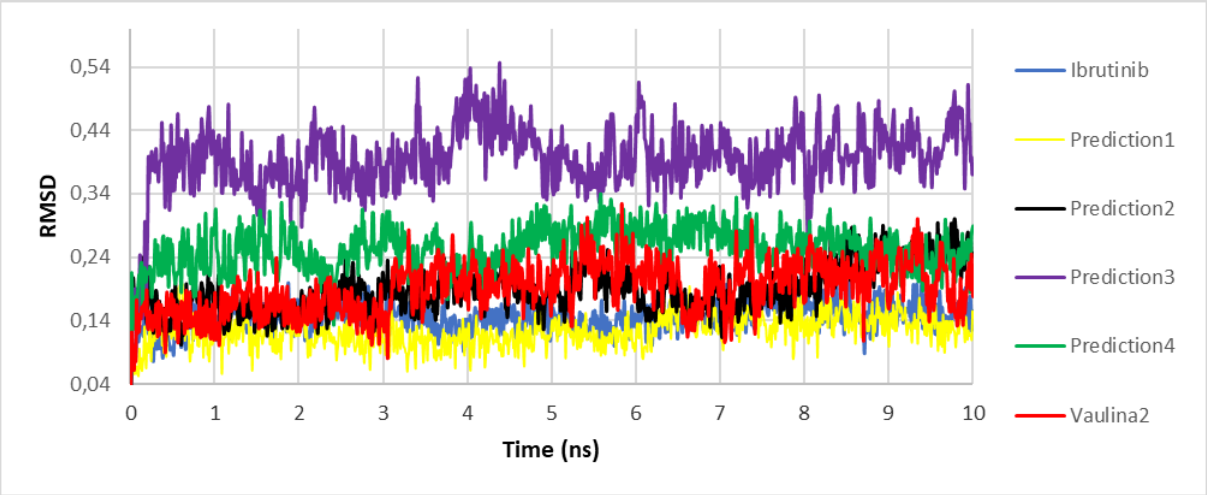

Figure 6. Comparison of RMSD profiles between ibrutinib and the predicted compounds.

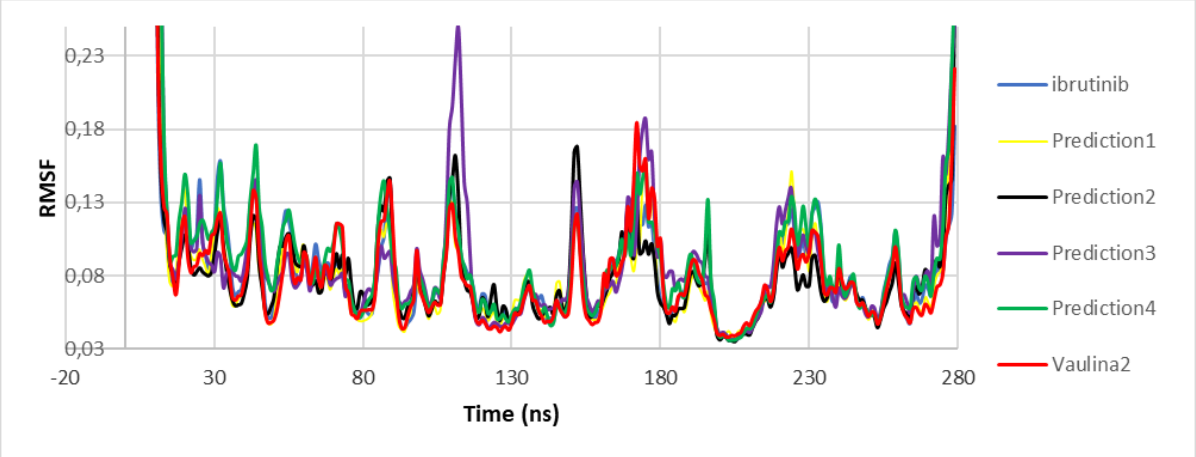

Figure 7. Comparison of RMSF profiles between ibrutinib and the predicted compounds.

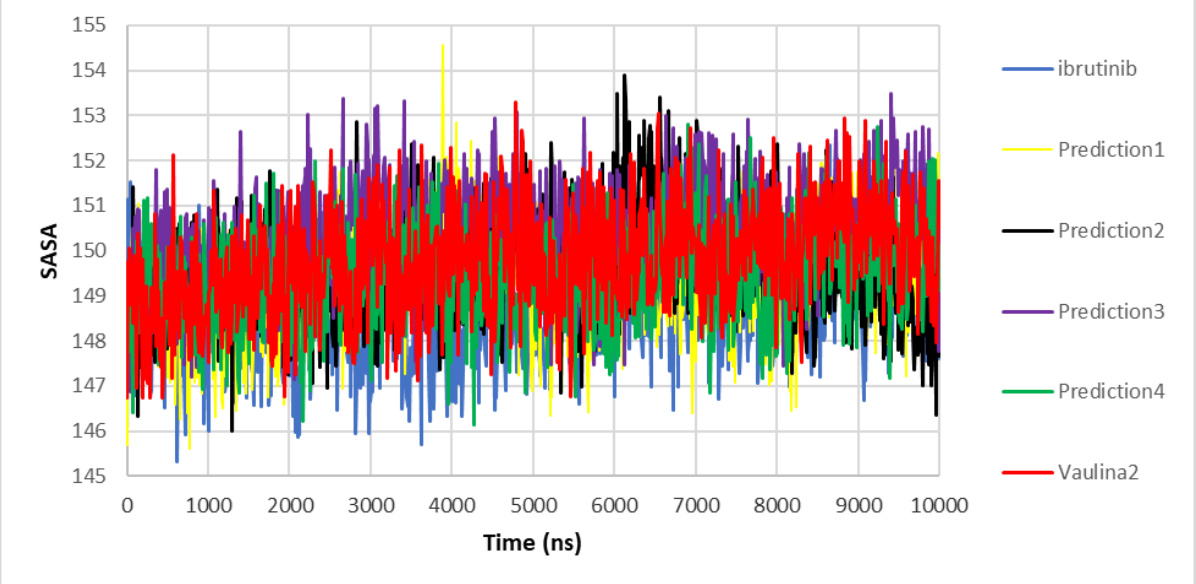

Figure 8. Comparison of SASA profiles between ibrutinib and the predicted compounds

Root-Mean-Square Fluctuation

RMSF measures the flexibility of individual amino acid residues in the receptor throughout the molecular dynamics simulation. A low RMSF value indicates that the residue maintains stable interactions with the ligand at the binding site, reflecting favorable conformational stability. In contrast, high RMSF values signify greater residue flexibility or limited participation in ligand binding, which may correspond to less stable interactions (Salo-Ahen et al., 2020). Figure 7 illustrates the RMSF profiles of the receptor in complex with ibrutinib and the predicted compounds. The fluctuation patterns were largely similar across all systems, except Prediction3, which displayed higher fluctuation at one amino acid residue.

SASA (Solvent Accessible Surface Area)

SASA quantifies the molecular surface area exposed to solvent molecules and is an important parameter in evaluating molecular interactions with aqueous environments. It is divided into two categories: 1) Polar regions, which involve atoms capable of forming hydrogen bonds or carrying partial charges; and 2) Non-polar regions, which involve hydrophobic atoms lacking charge or hydrogen-bonding capability (Anuar et al., 2020). Figure 8 presents the SASA plots derived from molecular dynamics simulations. The results indicate that the solvent interaction areas of the predicted compounds were nearly identical to those of ibrutinib, implying that ligand–solvent accessibility remained relatively constant among all complexes.

Hydrogen Bond Occupancy

Hydrogen bond occupancy analysis quantifies the persistence or frequency of hydrogen bond formation between ligand and receptor atoms throughout the simulation. A higher occupancy percentage indicates greater stability and stronger ligand–protein interactions, as hydrogen bonds play a crucial role in maintaining complex integrity (Zikri et al., 2021). The hydrogen bond occupancy data for ibrutinib and the predicted compounds (Prediction1, Prediction2, Prediction3, Prediction4, and Vaulina2) are presented in Table 6. The results demonstrate that ibrutinib exhibited a maximum hydrogen bond occupancy of 21.56%, forming a donor interaction with Asn146, suggesting that this residue plays a significant role in stabilizing the drug–receptor complex. Among the predicted compounds were 1) Prediction1 showed high occupancies of 39.82% with Asp159 and 42.81% with Thr94, where it acted as a donor in both cases, indicating that Asp159 and Thr94 are essential for its stability and binding activity; 2) Prediction2 demonstrated multiple hydrogen bond interactions, serving as a donor at 5.69% (Glu95) and 12.57% (Thr94), and as an acceptor at 7.78% (Thr94), 14.67% (Lys50), and 3.19% (Met97); 3) Prediction3 achieved its highest occupancy of 41.32% with Thr30, highlighting Thr30's critical role in maintaining ligand–receptor stability; 4) Prediction4 exhibited high occupancy values at 29.04% (Asp159), 9.88% (Lys50), 11.98% (Thr94), and 2.99% (Met97), demonstrating diverse stabilizing interactions; and 5) Vaulina2 reached its highest occupancy levels at 54.49% (Ser158) as an acceptor and 23.05% (Asp159) as a donor, emphasizing the importance of both residues in stabilizing its binding conformation. Overall, the hydrogen bond occupancy analysis indicates that the predicted compounds, particularly Prediction1, Prediction2, Prediction3, Prediction4, and Vaulina2, exhibited stronger and more stable hydrogen bonding interactions with the receptor's active site compared to ibrutinib, supporting their potential as promising BTK inhibitors in silico (see Table 6).

Table 6. Comparison of Hydrogen Bond Occupancy

Compound	Donor	Acceptor	Occupancy (%)	Compound	Donor	Acceptor	Occupancy (%)
Ibrutinib	Ibrutinib-side	Asp159-side	0.40	Prediction3	Prediction3-main	Thr30-main	41.32
	Ser158-side	Ibrutinib-side	0.30		Prediction3-side	Leu28-main	3.19
	Ibrutinib-side	Asn146-main	21.56		Asn104-side	Prediction3-side	0.4
	Ibrutinib-side	Ser158-side	0.50		Prediction3-main	Thr30-side	0.2
Prediction1	Prediction1-side	Asp159-side	39.82	Prediction4	Asp159-main	Prediction4-side	1.2
	Prediction1-side	Thr94-side	42.81		Prediction4-side	Asp159-side	29.04
	Thr94-side	Prediction1-side	1.6		Lys50-side	Prediction4-side	9.88
	Asp159-main	Prediction1-side	0.1		Prediction4-side	Thr94-side	11.98
	Ser158-side	Prediction1-side	1		Prediction4-side	Glu95-main	0.4
	Prediction1-side	Ser158-side	0.3		Met97-main	Prediction4-side	2.99
					Thr94-side	Prediction4-side	0.4
Prediction2	Thr94-side	Prediction2-side	7.78	Vaulina2	Ser158-side	Vaulina2-side	54.49
	Lys50-side	Prediction2-side	14.67		Vaulina2-main	Asp159-side	23.05
	Met97-main	Prediction2-side	3.19		Vaulina2-main	Ser158-side	0.9
	Prediction2-side	Glu95-side	5.69		Vaulina2-side	Leu28-main	0.1
	Prediction2-side	Thr94-side	12.57		Gly161-main	Vaulina2-side	0.2
					Asp159-main	Vaulina2-side	0.1

Table 7. MM-GBSA Binding Free-Energy Components for the Ligand–Receptor Systems

Energy Component (kcal/mol)	Ibrutinib	Prediction1	Prediction2	Prediction3	Prediction4	Vaulina2
van der Waals (VdW)	-51.51	-46.09	-45.68	-30.72	-38.15	-56.57
Electrostatic Energy (EEL)	-26.11	-22.34	-29.33	-81.18	-40.67	-110.53
Electrostatic Solvation Energy (EGB)	44.29	33.64	40.15	101.01	52.41	128.84
Non-polar Solvation Energy (ESURF	-7.11	-6.53	-6.47	-4.01	-5.78	-7.98
ΔG gas (VdW + EEL)	-77.62	-68.43	-75.01	-111.90	-78.82	-167.10
ΔG solv (EGB + ESURF)	37.18	27.10	33.68	97.00	46.62	120.86
ΔG total (VdW + EEL + EGB + ESURF)	-40.44	-41.33	-41.33	-14.90	-32.19	-46.24

MM-GBSA

The MM-GBSA calculation method provides a free energy (ΔG) value that reflects the binding affinity of a compound to a receptor. A lower ΔG value indicates a stronger binding affinity between the

compound and the receptor. Table 7 presents the MM-GBSA results. The total binding free energy (VdW + EEL + EGB + ESURF) for the reference drug ibrutinib was −40.44 kcal/mol. The corresponding values for the predicted compounds Prediction1, Prediction2, Prediction3, Prediction4, and Vaulina2 were −41.33, −41.33, −14.90, −32.19, and −46.24 kcal/mol, respectively. These results indicate that the total binding free energy (ΔG_total) of Prediction1, Prediction2, and Vaulina2 was lower than that of ibrutinib, suggesting more stable binding interactions and their potential as promising drug candidates in silico (see Table 7).

Conclusion

The analysis indicated that the docking results of the predicted compounds Vaulina2, Prediction1, Prediction2, Prediction3, and Prediction4 against the BTK receptor (PDB ID: 5P9J) exhibited greater stability compared to the reference drug ibrutinib, with Gibbs free energy (ΔG) values of –11.25, –12.50, –10.83, –10.74, and –10.63 kcal/mol, respectively. The ADMET prediction analysis further revealed that all five compounds satisfied the pharmacokinetic and toxicity criteria. The molecular dynamics analysis demonstrated that Vaulina2, Prediction1, and Prediction2 exhibited superior performance relative to ibrutinib, as reflected by favorable RMSD, RMSF, SASA, hydrogen bond occupancy, and MM-GBSA parameters.

Recommendations

Based on the docking, ADMET, and molecular dynamics analyses, it is recommended that Vaulina2, Prediction1, and Prediction2 be prioritized for further investigation as potential BTK inhibitors. These compounds demonstrated stronger binding affinity and higher stability than ibrutinib, along with favorable pharmacokinetic profiles. Future studies should focus on in vitro and in vivo validations to confirm their efficacy and safety profiles.

References

Smith, J. C., Hess, B., & Lindahl, E. (2015). GROMACS: High performance molecular simulations through multi-level parallelism from laptops to supercomputers. *SoftwareX*, 1–2, 19–25. https://doi.org/10.1016/j.softx.2015.06.001

Akinmoladun, F. O., Komolafe, T. R., Farombi, O. E., & Oyedapo, O. O. (2020). In silico prediction of anti-inflammatory activity of naturally occurring flavonoids. Tropical Journal of Natural Product Research, 4(12), 1078–1085. https://doi.org/10.26538/tjnpr/v4i12.9

Alov, P., Tsakovska, I., Pajeva, I. (2014) 'Computational Studies of Free Radical-Scavenging Properties of Phenolic Compounds', Curr Top Med Chem, 15(2), pp. 85-104. doi:10.2174/1568026615666141209143702

Alrumaihi, F., Khan, M.A., Babiker, A.Y. (2022) 'The Effect of Liposomal Diallyl Disulfide and Oxaliplatin on Proliferation of Colorectal Cancer Cells: In Vitro and In Silico Analysis', Pharmaceutics, 14(2), pp. 236. doi:10.3390/pharmaceutics14020236

Anoor, P.K., Yadav, A.N., Rajkumar, K, et al. (2022) 'Methanol extraction revealed anticancer compounds Quinic Acid, 2(5H)-Furanone and Phytol in Andrographis paniculata', Mol Clin Oncol, 17(5), pp. 1-13. doi:10.3892/mco.2022.2584

Anuar, N. F. S. K., Wahab, R. A., Huyop, F., et al. (2020) 'Molecular docking and molecular dynamics simulations of a mutant Acinetobacter haemolyticus alkaline-stable lipase against tributyrin', J Biomol Struct Dyn, 39(6), pp.2079-2091. doi:10.1080/07391102.2020.1743364

Bazmi, S., Wallin, S. (2024) 'Comparing effects of attractive interactions in

crowded systems: nonspecific, hydrophobic, and hydrogen bond interactions', PeerJ Phys Chem, doi:10.7717/peerj-pchem.31

BIOVIA, Dassault Systèmes. (2021). Discovery Studio Modeling Environment, Release 2021. San Diego: Dassault Systèmes.

Bissantz, C., Kuhn, B., Stahl, M. (2010) 'A Medicinal Chemist's Guide to Molecular Interactions', J Med Chem, 53(14), pp. 5061-5084. doi:10.1021/jm100112j

Bobe, G., Zhang, Z., Kopp, R., Garzotto, M., Shannon, J., Takata, Y. (2020) 'Phytol and its metabolites phytanic and pristanic acids for risk of cancer: current evidence and future directions', Eur J Cancer Prev, 29(2), pp. 191-200. doi:10.1097/CEJ.0000000000000534

Carugo, O. and Djinovic, C. K. (2013) 'Half a century of Ramachandran plots', Acta Crystallogr Sect D Biol Crystallogr, 69(8), pp.1333-1341. doi:10.1107/s090744491301158x

Chasani, M. (2002) 'Synthesis Of Calanone Derivates And Biology Activity Test', thesis.

Chasani, M., Vaulina, E., Iswanto, P., Hanafi, M. (2008) 'Sintesis Senyawa Etilendiamin Kalanon Melalui Reaksi Adisi Gugus Etilendiamin Terhadap Ikatan Rangkap C7-8 Dan Uji Aktivitas Antileukemia Terhadap Sel Leukemia L1210', Molekul, 3(1). doi:10.20884/1.jm.2008.3.1.43

Chasani, M., Vaulina, E., Iswanto, P., Rahayu, Y. (2010) 'Hidrasi Ikatan Rangkap C7-8 Senyawa Kalanon Dan Uji Sitotoksisitasnya Terhadap Sel Leukemia L1210', Molekul, 5(1), pp. 41. doi:10.20884/1.jm.2010.5.1.75

Chasani, M., Iswanto, P., Vaulina, E., Putra, W. S., Hanafi, M. (2011) 'Semi Sintesis Senyawa 2,4,6-Trinitrofenilhidrazon Kalanon Dan Uji Aktivitas Terhadap Sel Leukimia L1210', J Mol, 6(2). doi:http://dx.doi.org/10.20884/1.jm.2011.6.2.94

Di Francia, R., Crisci, S., De Monaco, A., et al. (2021) 'Response and toxicity to cytarabine therapy in leukemia and lymphoma: From dose puzzle to pharmacogenomic biomarkers', Cancers, 13(5), pp.1-39. doi:10.3390/cancers13 050966

Ding, X., Herzlich, A. A., Bishop, R., Tuo, J., Chan, C.C. (2008) 'Ocular toxicity of fludarabine: a purine analog', Neuron, 61(1), pp. 1-7. doi:10.1586/17469899.3.1.97

Fanfrlík, J., Bronowska, A. K., Řezáč, J., & Přenosil, O. (2010). "A reliable docking/scoring scheme based on the semiempirical quantum mechanical PM6-DH2 method accurately covering dispersion and H-bonding: HIV-1 protease with 22 ligands'. The Journal of Physical Chemistry B, 114(39), 12666–12678. https://doi.org/10.1021/jp1032965

Gliszczyńska, A., Dancewicz, K., Gabryś, B., Świtalska, M., Wietrzyk, J., Maciejewska, G. (2021) 'Synthesis of novel phytol-derived γ-butyrolactones and evaluation of their biological activity', Sci Rep, 11(1), pp. 1-14. doi:10.1038/s41598-021-83736-6

Hafez, H. A., Soliaman, R. M. and Bilal, D. et al. (2019) 'Early Deaths in Pediatric Acute Leukemia : A Major Challenge in Developing Countries', J Pediatr Hematol Oncol, 41(4), pp. 261-266. doi:10.1097/MPH.0000000000001408

Hanwell, M. D., Curtis, D. E., Lonie, D. C., Vandermeersch, T., Zurek, E., & Hutchison, G. R. (2012). Avogadro: an advanced semantic chemical editor, visualization, and analysis platform. Journal of Cheminformatics, 4, 17. https://doi.org/10.1186/1758-2946-4-17

Harris, K.M., Majmundar, M.K. and Becker, T. (2021) 'High and Rising Mortality Rates among Working-Age Adults'. doi:10.17226/25976

Hevener, K. E., Zhao, W., Ball, D. M., Babaoglu, K., Qi, J., White, S. W., & Lee, R. E. (2009). Validation of molecular docking programs for virtual screening against dihydropteroate

synthase. Journal of Chemical Information and Modeling, 49(2), 444–460. https://doi.org/10.1021/ci800293n

Humphrey, W., Dalke, A., & Schulten, K. (1996). VMD: Visual molecular dynamics. Journal of Molecular Graphics, 14(1), 33–38. https://doi.org/10.1016/0263-7855(96)00018-5

Iswanto, P., Chasani, M., Harjono, H., Tahir, I., Hanafi, M., Vaulina, Y. D. E. (2011) 'Novel Design of Calanone Derivatives As Anti-Leukemia Compounds Based on Quantitative Structure-Activity Relationship Analysis', Indones J Chem, 11(1), pp. 31-36. doi:10.22146/ijc.21416

Kruk, M. E., Gage, A. D., Joseph, N. T., Danaei, G., García-Saisó, S., Salomon, J. A. (2018) 'Mortality due to low-quality health systems in the universal health coverage era: a systematic analysis of amenable deaths in 137 countries', Lancet, 392 (10160), pp. 2203-2212. doi:10.1016/S0140-6736(18)31668-4

Khan, S.U., Fatima, K., Aisha, S., Malik, F. (2024) 'Unveiling the mechanisms and challenges of cancer drug resistance', Cell Commun Signal, 22(1), pp. 1-26. doi:10.1186/s12964-023-01302-1

Kolina, J., Sumiwi, S. A., Levita, J. (2019) 'Mode Ikatan Metabolit Sekunder di Tanaman Akar Kuning (Arcangelisia flava L.) dengan Nitrat Oksida Sintase', FITOFARMAKA J. Ilm. Farm, 8(1), pp. 45-52. doi:10.33751/jf.v8i1.1171

Karplus, M. (2002) 'Molecular dynamics simulations of biomolecules', Acc Chem Res, 35(6), pp.321-323. doi:10.1021/ar020082r

Lagunin, A., Stepanchikova, A., Filimonov, D., & Poroikov, V. (2000). PASS: prediction of activity spectra for biologically active substances. Bioinformatics, 16(8), 747–748. https://doi.org/10.1093/bioinformatics/16.8.747

Lyengar, V., Mukkamalla, S. K. R., and Shimanovsky A. (2023) 'Leukimia', https://www.ncbi.nlm.nih.gov/books/NBK56 0490/

Lei, Z. N., Tian, Q. and Teng, Q. X. (2023) 'Understanding and targeting resistance mechanisms in cancer', MedComm, 4(3), pp. 1-38. doi:10.1002/mco2.265

Leelananda, S.P., Lindert, S. (2016) 'Computational methods in drug discovery', Beilstein J Org Chem, 12, pp. :2694-2718. doi:10.3762/bjoc.12.267

Madhavi, S. G., Adzhigirey, M., Day, T., Annabhimoju, R., Sherman, W. (2013) 'Protein and ligand preparation: Parameters, protocols, and influence on virtual screening enrichments', J Comput Aided Mol Des, 27(3), pp. 221-234. doi:10.1007/s10822-013-9644-8

Mardianingrum, R., Endah, S. R. N., Suhardiana, E., Ruswanto, R., Siswandono, S. (2021) 'Docking and molecular dynamic study of isoniazid derivatives as anti-tuberculosis drug candidate', Chemical Data Collections, doi:10.1016/j.cdc. 2021.100647

Meng, X. Y., Zhang, H. X., Mezei, M., Cui, M. (2022) 'Molecular Docking: A Powerful Approach for Structure Based Drug Discovery', Int J Pharm Sci Rev Res, 77(2), pp. 146-157. doi:10.47583/ijpsrr.2022.v77i02.029

Monika, M., Richa, R., Dhingra, N. (2016) '3-Thiocyanato- 1 H - indoles as potential anticancer agents : Two dimensional quantitative structure activity relationship study', Int J Pharm Chem Anal, 3(4), pp. 198-204. doi:10.18231/2394-2797.2016.0003

Mohanty, M. and Mohanty, P. S. (2023) 'Molecular Docking In Organic, Inorganic, and Hybrid Systems: A Tutorial Review', Monatshefte fur Chemie-Chemical Monthly, 154(7), pp. 683-707. doi:10.1007/s00706-023-03076-1

Morris, G. M., Huey, R., Lindstrom, W., Sanner, M. F., Belew, R. K., Goodsell, D. S., & Olson, A. J. (2009). AutoDock4

and AutoDockTools4: Automated docking with selective receptor flexibility. Journal of Computational Chemistry, 30(16), 2785–2791. https://doi.org/10.1002/jcc.21256

Muttaqin, F. Z. (2019) 'Molecular Docking and Molecular Dynamic Studies of Stilbene Derivative Compounds As Sirtuin-3 Histone Deacetylase Inhibitor on Melanoma Skin Cancer and Their Toxicities Prediction', J Pharmacopolium, 2(2), pp.112-121. doi:10.36465/jop.v2i2.489

Najibi, S. M., Maadooliat, M., Zhou, L., Huang, J. Z., Gao, X. (2017) 'Protein Structure Classification and Loop Modeling Using Multiple Ramachandran Distributions', Comput Struct Biotechnol J, 15, pp. 243-254. doi:10.1016/j.csbj.2017. 01.011

Octavinna, N., Zuhrotun, A, Yohana, C. A. (2018) 'Aktivitas Senyawa Aktif Michelia Champaca Sebagai Inhibitor Topoisomerase Antikanker', Farmaka, 16(3), pp. 185-195.

Phillips, N. S., Duke, E. S., Hannah-Lise, Schofield,, T., Ullrich, N. J. (2021) 'Neurotoxic Effects of Childhood Cancer Therapy and Its Potential Neurocognitive Impact', Neurocognitive Outcomes Surviv Pediatr Cancer, 39(16), pp. 752-1765. doi:10.1200/JCO.20.02533

Pires, D. E. V., Blundell, T. L., Ascher, D. B. (2015) 'pkCSM: Predicting Small-Molecule Pharmacokinetic and Toxicity Properties Using Graph-Based Signatures', J Med Chem, 58, pp.4066-4072. doi:10.1021/acs.jmedchem.5b00104

Pettersen, E. F., Goddard, T. D., Huang, C. C., Couch, G. S., Greenblatt, D. M., Meng, E. C., & Ferrin, T. E. (2004). UCSF Chimera—A visualization system for exploratory research and analysis. Journal of Computational Chemistry, 25(13), 1605–1612. https://doi.org/10.1002/jcc.20084

Purnawan, P. P. (2022) 'Teori Dan Tutorial Molecular Docking Menggunakan AutoDock Vina', 1st, Banyumas : Wawasan Ilmu

Purnomo, H. (2011) 'Kimia Komputasi: Molecular Docking Plants [Protein-Ligand-Ant-System], 1st, Yogyakarta. Pustaka Pelajar.

Purnomo H. (2019) 'Molecular Docking Parasetamol Dan Analognya Menggunakan PLANTS (Protein Ligand ANT System)', Yogyakarta : Adhi Publishing.

Rachmania, R. A., Supandi, S., Cristina, F. A. D. (2016) 'Analisis Penambatan Molekul Senyawa Flavonoid Buah Mahkota Dewa (Phaleria macrocarpa (Scheff.) Boerl.) pada Reseptor alfa-Glukosidase sebagai Antidiabetes', PHARMACY, 13(2), pp.239-251. Doi: https://jurnalnasional.ump.ac.id/index.php/PHARMACY/article/view/1260

Rachmania, R.A. (2019) 'Validasi Protokol Skrining Virtual dan Analisis Interaksi Inhibitor Antiproliferasi Sel Kanker Berbasis Bahan Alam Terhadap Reseptor Cyclin-Dependent Kinase 4', Media Farm. J. Ilmu Farm, 16(1), pp. 21. doi:10.12928/mf.v16i1.12101

Ramadhani, A. N., Wahyudi, S. T., and Lestari, D. P. (2021) 'Langkah Lengkap Drug Discovery Menggunakan Molecular Docking', 1st. Global Science.

Remesh, A. (2012) 'Toxicities of anticancer drugs and its management', Int J of Basic Clinical Pharmacology, 1(1): pp. 2-12. doi:10.5455/2319-2003.ijbcp000812

Reynaldi, M. A., Setiawansyah, A. (2022) 'Potensi anti-kanker payudara tanaman songga (Strychnos lucida R.Br): Tinjauan interaksi molekuler terhadap reseptor estrogen-α in silico', Sasambo J Pharm, 3(1), pp. 30-35. doi:10.29303/sjp.v3i1 .149

Ruswanto, R., Nofianti, T., Mardianingrum, R., Kesuma, D., Siswandono. (2022) 'Design, molecular docking, and molecular dynamics of thiourea-iron (III) metal complexes as NUDT5 inhibitors for breast cancer treatment', Heliyon, 8(9), doi:10.1016/j.heliyon.2022.e10694

Ruswanto, R., Mardianingrum, R., Nofianti, T., Pratita, A. T. K., Naser, F. M., Siswandono, S. (2023) 'Design and computational study of the thiourea–cobalt(III) complex as an anticancer candidate', J Pharm Pharmacogn Res, 11(3), pp.499-516. doi:10.56499/jppres23.1622_11.3.499

Salo-Ahen, O. M. H., Alanko, I., Bhadane, R., et al. (2020) 'Molecular Dynamics Simulations in Drug Discovery and Drug Delivery. Processes', 71(9), pp.1-60. doi:10.1007/978-3-030-36260-7_10

Santos, D. S. dos and Goldenberg, R. C. dos. (2018) 'Doxorubicin-Induced Cardiotoxicity: from Mechanisms to Development of Efficient Therapy', In: IntechOpen, 11, pp. 3-24. doi://dx.doi.org/10.5772/intechopen.79588

Sari, I. W., Junaidin, J., Pratiwi, D. (2020) 'Studi Molecular Docking Senyawa Flavonoid Herba Kumis Kucing (Orthosiphon stamineus B.) pada reseptor α-glukosidase sebagai antidiabetes tipe 2', J Farmagazine, 7(2), pp.54. doi:10.47653/farm.v7i2.194

Sagitasa, S., Elizabeth, K., Sulaeman, L. I., et al. (2021) 'Studi In Silico Senyawa Aktif Daun Singawalang (Petiveria alliacea)', Chim Nat Acta, 9(2), pp. 58-66. doi:https://doi.org/10.24198/cna.v9.n2.34083

Sinha, S., Tam, B., Wang, S. M. (2023) 'Applications of molecular dynamics simulation in nanomedicine', Nanomedicine Technol Appl, 844(12), pp.1-17. doi:10.1016/B978-0-12-818627-5.00007-5

Susanti, N. M. P., Laksmiani, N. P. L., Noviyanti, N. K. M., Arianti, K. M., Duantara, I. K. (2019) 'Molecular Docking Terpinen-4-ol sebagai Antiinflamasi pada Aterosklerosis secara in Silico', J Kim, 13(2), pp. 221-228. doi:10.24843/jchem.2019.v13.i02.p16

Tarmizi SN. Kemenkes dan Viva Anak Kanker Indonesia Sepakat Perkuat Kerja Sama. Biro Komunikasi dan Pelayanan Publik, Kementerian Kesehatan RI. Published 2024. https://sehatnegeriku.kemkes.go.id/baca/umum/20240115/5544773/kemenkes-dan-viva-anak-kanker-indonesia-sepakat-perkuat-kerja-sama/

Trott, O., Olson, A. J. (2010) 'AutoDock Vina: Improving the speed and accuracy of docking with a new scoring function, efficient optimization, and multithreading', J Comput Chem, 31(2), pp. 455-461. doi:10.1002/jcc.21334

Tsai, C. J., Wang, S. S., Ou, Y.C. (2014) 'Cyclophosphamide-induced intractable hemorrhagic cystitis treated with hyperbaric oxygenation and intravesical sodium hyaluronate', Urol Sci, 25(4), pp. 155-157. doi:10.1016/j. urols.2014.03.001

Vaulina, Y. D. E., Chasani, M., Abdulghani, M. (2012) 'Hubungan Kuantitatif Struktur-Aktivitas (HKSA) Antikanker Senyawa Turunan Kalanon Dengan Metode Semi Empiris PM3 (Parameterized Model 3)', Molekul, 7(2), pp.130. doi:10.20884/1.jm.2012.7.2.115

Van, G. W., Bakowies, D., Bürgi, R., et al. (2001) 'Molecular dynamics simulation of biomolecular systems', Chimia, 55(10), pp.856-860. doi:10.2533/chimia.2001.856

Wang, L., Friesner, R. A., Berne, B. J. (2008) 'Competition of electrostatic and hydrophobic interactions between small hydrophobes and model enclosures', J Phys Chem B, 23(1), pp.1-7. doi: https://doi.org/10.1021/jp100772w.

Wicaksono, A., Raihandhany, R., Zen, T. V., da Silva, J. A. T., Agatha, A., Cristy, G. P., Ramadhan, A. T. K., & Parikesit, A. A. (2022). Screening Rafflesia and Sapria metabolites using a bioinformatics approach to assess their potential as drugs. Philippine

Journal of Science, 151(5), 1771–1791.

Yunarto, N., Sulistyaningrum, N. (2017) 'Quantitative Analysis of Bioactive Compounds In Extract and Fraction of Star Fruit (Averrhoa carambola L.) Leaves Using High Performance Liquid Chromatography', J Kefarmasian Indones, 7(1), pp. 26-33. doi:10.22435/jki.v7i1.5605.26-33

Yuliana, A., Rahmiyani, I., Kartika, C. (2021) 'Molecular Docking and Molecular Dynamics Simulation using Monascus sp. as a Candidate Cervical Cancer Drug', J Trop Pharm Chem, 5(4), pp. 396-405. https://jtpc.farmasi.unmul.ac.id

Young, D. C. (2009) 'Computational Drug Design : A Guide For Computational And Medicinal Chemists', New Jersey : John Willey & Sons, Inc.

Zikri, A. T., Pranowo, H. D., Haryadi, W. (2021) 'Stability hydrogen bond occupancy analysis and binding free energy calculation from flavonol docked in DAPK1 active site using molecular dynamic simulation approaches', Indones J Chem, 21(2), pp.383-390. doi:10.22146/ijc.56087.